Sintering Shrinkage and Microstructure Evolution during Densification of a Martensitic Stainless Steel

D.C. Blaine*, Y. Wu, C.E. Schlaefer, B. Marx, and R.M. German
The Pennsylvania State University

September 4, 2003

Abstract

The densification and microstructural evolution of 17-4PH stainless steel is investigated by means of dilatometry and quenching experiments. The densification kinetics are explained by identifying the microstructure with phase changes for this alloy at key points along the densification curve. Sintering experiments conducted in pure hydrogen, and in hydrogen-nitrogen atomspheres illustrate the austenitic stabilizing effect that nitrogen has on this martensitic stainless steel. This is shown to have a significant affect on the densification kinetics.

1 Introduction

17-4PH stainless steel is a precipitation-hardenable martensitic stainless steel with high strength and good corrosion resistance. It is an attractive material for powder injection molding (PIM), especially for intricately shaped components such as medical instruments [1, 2]. This alloy has drawn some interest in PIM research circles, however most studies have focussed on the effects of debinding, sintering and heat-treatment on the final properties [3]-[11]. Generally 17-4PH can be sintered to full density with good final properties if the sintering occurs in vacuum or in a pure hydrogen atmosphere [3, 4, 6]. Reported sintering temperatures for high density range from $1250\,^{\circ}\mathrm{C}$ to $1390\,^{\circ}\mathrm{C}$. Residual carbon content from debinding has a highly influential effect on final density, corrosion resistance and microstructure [6, 8].

Despite all these studies, the densification kinetics of 17-4PH have not been thoroughly studied before. Injection molded 17-4PH stainless steel is know to have uniformly distributed δ-ferrite in a martensitic microstructure, however the influence that this phase has on densification has, as yet, remained unexplored. By performing quenching experiments at key points along the shrinkage curve, the microstructure can be frozen in time. By examining these key point microstructures, correlation can be drawn between present phases and densification kinetics, giving major insight into the manner in which this alloy sinters.

These results will allow researchers to design optimal sinter cycles, using the fast diffusion paths of favourable phases. They also offer invaluable insight for development of the continuum laws of sintering, used in finite element computer models of sintering. The continuum laws of sintering rely heavily on the apparent viscosity of the sintering body at any given point during the densification path [12]. As the apparent viscosity is directly linked to diffusion coefficients [13, 14], which vary between phases, knowledge of the present phases and their influence on densification is integral to the creation of an intelligent sinter model.

2 Experimental Procedure

Samples for dilatometer and quenching studies were consolidated from ATMIX water-atomized 17-4PH stainless steel powder. Powder characteristics are given in Table 1.

Table 1: Powder characteristics of ATMIX water-atomized 17-4PH stainless steel

Tap density	4.30 $\mathrm{g/cm^3}$
Pycnometer density	7.66 $\mathrm{g/cm^3}$
Particle size:	
D_{10}	3.4 $\mu\mathrm{m}$
D_{50}	9.2 $\mu\mathrm{m}$
D_{90}	23.4 $\mu\mathrm{m}$

For the injection-molded samples, a water-based agar binder was used to compound the feedstock with 55 vol % solids loading. Water-based agar feedstocks do not need solvent debinding as the water evaporates out of the injection-molded sample. Thermal debinding at $450\,^{\circ}\mathrm{C}$ for 2 hours in hydrogen was conducted in a retort furnace. Samples ($15\ \mathrm{mm}$ height, 7.6 x 7.6 mm cross-section) were cut from the gauge of debound tensile bars.

Die-compacted samples were compacted without lubricant in a uniaxial laboratory press to a pressure of $35\ \mathrm{MPa}$. The green density of the die-compacted cylinder samples (12.8 $\mathrm{mm}\ \phi$, 12.9 mm height) was 71% theoretical.

Sintering shrinkage was measured using an Anter vertical pushrod dilatometer. Two atmospheres were investigated: pure hydrogen (dewpoint $-75\,^{\circ}\mathrm{C}$) and 60:40 vol % hydrogen:nitrogen.

A vertical quench furnace was used for the quenching studies. Samples were sintered to the key points along the sinter cycle, and then dropped through a trapdoor into a room temperature water bath to quench. The same atmospheres as used for the dilatometer studies were used for the quenching studies.

The sinter cycle followed for all experiments was $10\,^{\circ}\mathrm{C/min}$ to $1010\,^{\circ}\mathrm{C}$ with a 1 hour hold at this temperature, and then $10\,^{\circ}\mathrm{C/min}$ to $1365\,^{\circ}\mathrm{C}$ with another 1 hour hold at this temperature. Then the sample was cooled at $10\,^{\circ}\mathrm{C/min}$ to room temperature. The hold at $1010\,^{\circ}\mathrm{C}$ is for complete removal of the binder.

Sintered density was measured using the Archimedes density measurement technique. Samples were prepared for microstructural evaluation by cutting, mounting, grinding and polishing to a 0.3 μm surface finish using standard metallographic procedures. A Kalling's reagent (2 g $CuCl_2$, 40 ml HCl, 60 ml ethanol and 40 ml H_2O) was used for etching.

3 Results

Figure 1 shows the shrinkage results from dilatometer runs for both PIM and die-compacted samples sintered in both H_2 and H_2:N_2 atmospheres. The temperature profile is included on the secondary axis to aid in the analysis of the shrinkage results. Figure 2 shows the shrinkage rate results, calculated from the dilatometer shrinkage by taking time averages of the rate over 10 data points at a time, for the same experiments.

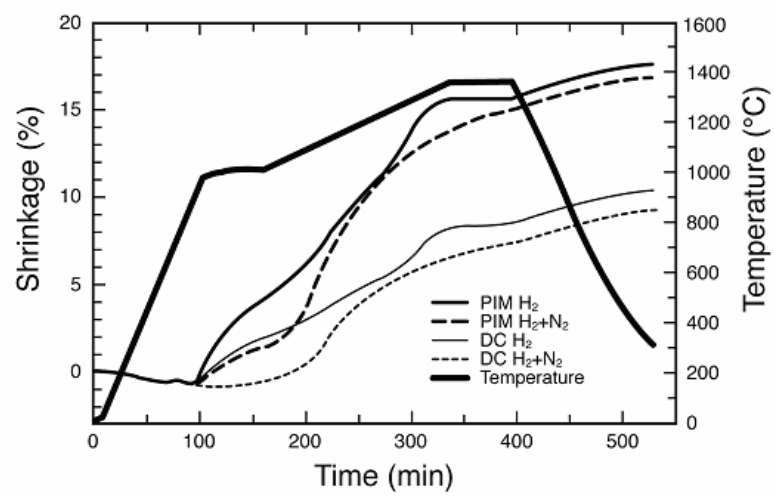

Figure 1: Dilatometer shrinkage results for PIM and die-compacted samples sintered in H_2 and H_2:N_2. The thermal profile of the sinter cycle is also shown.

By examining these graphs some significant information and key points can be isolated. Firstly, up to $900\,^{\circ}$C thermal expansion dominates, however there is a small peak in the shrinkage and shrinkage rate around $720\,^{\circ}$C. For aid in the analysis, the peaks in the shrinkage rate are numbered as they indicate key points in the sinter cycle as will be shown. The peak around $720\,^{\circ}$C is labelled Peak I.

Sintering shrinkage starts around $900\,^{\circ}$C which indicates the beginning of the intermediate stage of sintering. Around this point the shrinkage rate experiences its second peak, Peak II. However, during the ramp to and hold at $1010\,^{\circ}$C the H_2:N_2 samples show definite retardation of shrinkage compared to the H_2 samples.

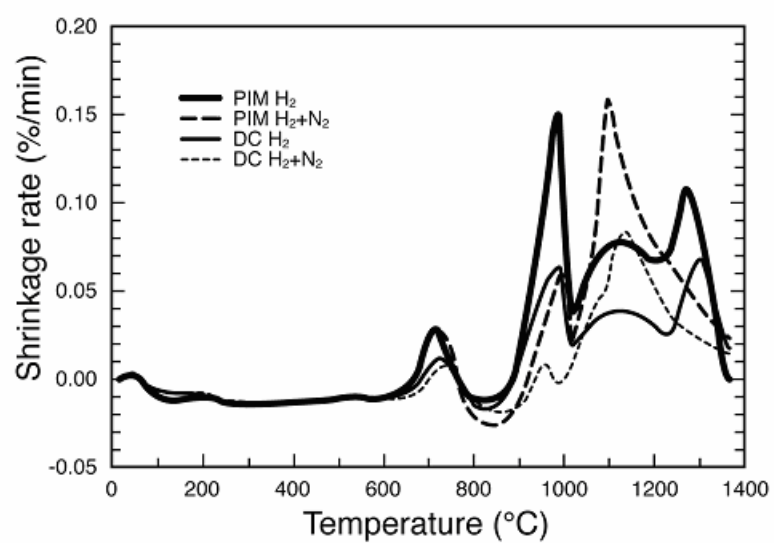

Figure 2: Shrinkage rate results showing peaks for PIM and die-compacted samples sintered in H_2 and H_2:N_2.

As soon as the temperature starts ramping up again, after the $1010\,^{\circ}\mathrm{C}$ hold, there is a sharp increase in the shrinkage rate. This peak is labelled Peak III. This sharp increase in shrinkage rate is expected with the associated heating ramp. It is a characteristic of sintering that during an isothermal hold the shrinkage rate will gradually deaccelerate, and that any increase in temperature past this isothermal temperature will boost the shrinkage rate [15]. It is also understandable that the H_2:N_2 samples would experience a sharper peak in shrinkage rate than the H_2 samples, as the fact that their shrinkage rate was retarded during the $1010\,^{\circ}\mathrm{C}$ hold left them at a lower density with a higher potential for sintering at the beginning of the second ramp.

The H_2:N_2 samples almost catch up to the H_2 samples around $1200\,^{\circ}\mathrm{C}$, but right at this point the H_2 samples experience another peak in sintering, labelled Peak IV. As there is no change in heating rate at this point, and this change in shrinkage rate is seen only in the H_2 samples, there is no external reason apparent for this peak. This makes Peak IV of particular interest in this study. It is, in fact, this peak that springboards the H_2 samples to their maximum shrinkage and densification levels, before they have even reached their final sintering temperature of $1365\,^{\circ}\mathrm{C}$. The H_2:N_2 samples however continue to sinter steadily up the final hold temperature. Their shrinkage rate starts to wane during the isothermal hold, as is characteristic of sintering.

Table 2 lists the peaks as described in the above description of the sintering shrinkage evolution of the samples. It is worthwhile mentioning that the overall shrinkage of ~15% for the PIM samples, and ~8% for the die-compacted samples both correlate to similar final densities for similar sintering atmospheres. This can be explained by noting that the green density for the PIM samples was 55% theoretical, while for the die-compacted samples it was 71% theoretical thus

less shrinkage is needed in the die-compacted samples to reach full density. Figure 3 shows the density evolution of the samples at various points along the sinter cycle. Here it can be seen that the consolidation technique does not significantly influence the final density, whereas the sintering atmosphere certainly does.

Table 2: Position of shrinkage rate peaks during sintering

Sample	Peak I	Peak II	Peak III	Peak IV
PIM in H_2	$716\,^{\circ}\mathrm{C}-721\,^{\circ}\mathrm{C}$	$960\,^{\circ}\mathrm{C}-992\,^{\circ}\mathrm{C}$	$1116\,^{\circ}\mathrm{C}-1140\,^{\circ}\mathrm{C}$	$1271\,^{\circ}\mathrm{C}-1282\,^{\circ}\mathrm{C}$
PIM in H_2:N_2	$727\,^{\circ}\mathrm{C}-735\,^{\circ}\mathrm{C}$	$988\,^{\circ}\mathrm{C}-996\,^{\circ}\mathrm{C}$	$1103\,^{\circ}\mathrm{C}-1106\,^{\circ}\mathrm{C}$	–
die-compacted in H_2	$725\,^{\circ}\mathrm{C}-730\,^{\circ}\mathrm{C}$	$964\,^{\circ}\mathrm{C}-996\,^{\circ}\mathrm{C}$	$1112\,^{\circ}\mathrm{C}-1143\,^{\circ}\mathrm{C}$	$1295\,^{\circ}\mathrm{C}-1308\,^{\circ}\mathrm{C}$
die-compacted in H_2:N_2	$728\,^{\circ}\mathrm{C}-738\,^{\circ}\mathrm{C}$	$955\,^{\circ}\mathrm{C}-964\,^{\circ}\mathrm{C}$	$1130\,^{\circ}\mathrm{C}-1143\,^{\circ}\mathrm{C}$	–

4 Microstructural Analysis

To investigate Peak I around $720\,^{\circ}\mathrm{C}$, the microstructure of the powder was analyzed before sintering and after quenching from $780\,^{\circ}\mathrm{C}$. It is not necessary to show the difference in microstructure between consolidation methods or sintering atmospheres at this point, as microstructurally the samples all experience similar behaviour. Before sintering the powder shows a solidified martensitic structure, Figure3, whereas the samples quenched from $780\,^{\circ}\mathrm{C}$ show a solidified martensitic lath structure, Figure 3. This is evidence of austenizing, and indicates that Peak I is associated with the phase transformation from low density bct martensite (α) $\rightarrow$ higher density fcc austenite (γ) [16].

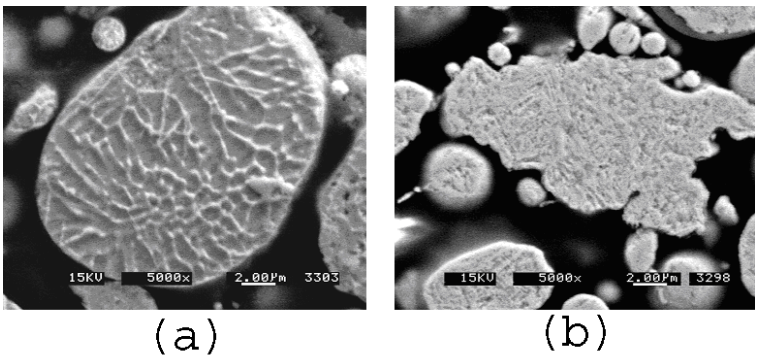

Figure 3: Microstructures of the powder before sintering (a) and after quenching from $780\,^{\circ}\mathrm{C}$ (b).

Peak II and III occur in both the die-compacted and PIM samples between $900\,^{\circ}\mathrm{C}$ and $1200\,^{\circ}\mathrm{C}$, and for both sintering atmospheres. The difference in behaviour between the consolidation methods and sintering atmospheres is only seen in the relative amplitude of the shrinkage rate peaks. For this reason, the microstructures shown in this paper are only for the die-compacted samples.

A more thorough study involving discussion of the effect of residual binder on the microstructure of the PIM samples is given elsewhere by Wu *et al* [16, 17]. Figure 4 shows the aforementioned die-compacted microstructures for the samples sintered in both pure H_2 and the H_2:N_2 mixture. It can be seen that the presence of nitrogen significantly affects the densification in this temperature range, $900\,^{\circ}\mathrm{C}$ to $1200\,^{\circ}\mathrm{C}$. The H_2:N_2 sintered samples also exhibit different phase presence than the H_2 samples. X-ray diffraction performed on the samples quenched from $1000\,^{\circ}\mathrm{C}$ indicates that the presence of nitrogen correlates with more retained austenite (γ) [16]. A typical austenite stabilizer, the interstitial nitrogen can strongly retard the austenite $\rightarrow$ martensite transformation [2].

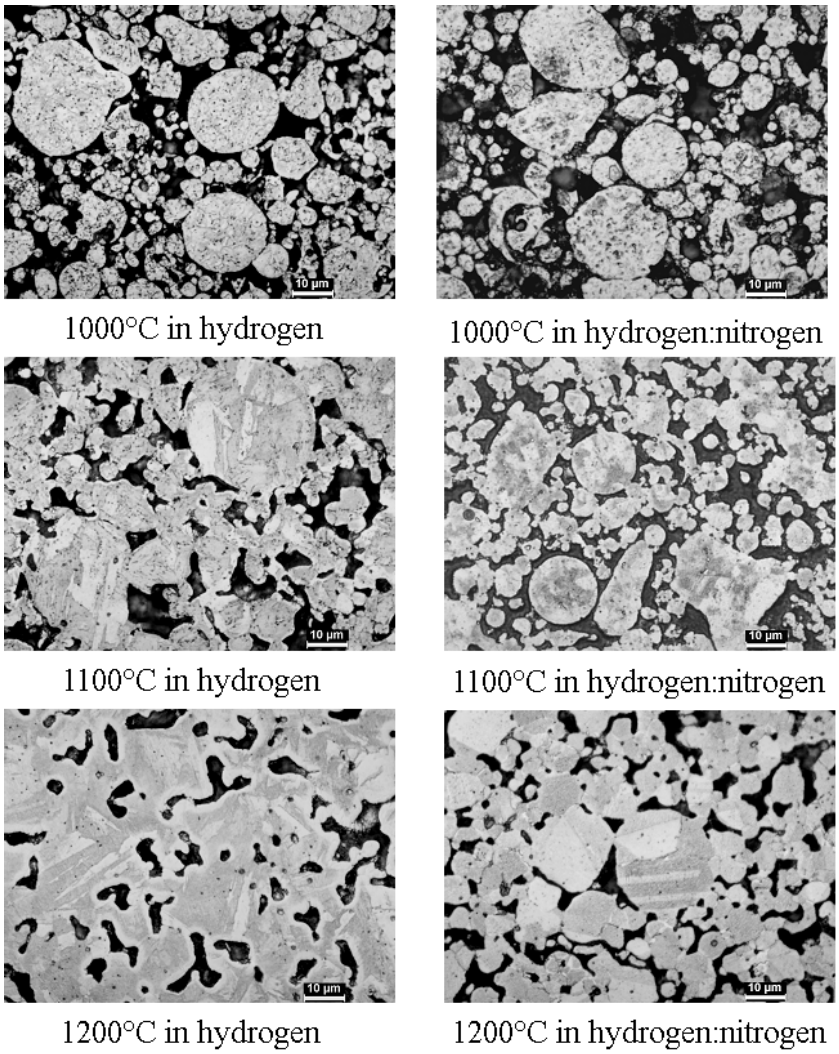

Figure 4: Quenched microstructures of die-compacted samples between $900\,^{\circ}\mathrm{C}$ and $1200\,^{\circ}\mathrm{C}$.

The fourth peak around 1220 °C is only present in the samples sintered in hydrogen. The difference between the behaviour of the die-compacted and PIM samples does not significantly affect the microstructure, so again only the die-compacted sample microstructures are shown in Figure 5. The PIM samples are discussed at length in the previously mentioned studies by Wu *et*

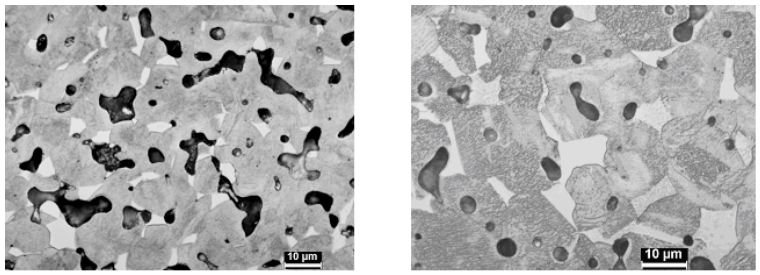

Figure 5: Microstructures of die-compacted samples quenched from indicated temperatures

al. The sample quenched from 1260 °C shows a considerable amount of new phase (light in colour) formed in the austenite (transformed to martensite during quenching) phase. The new phase grows along the grain and pore boundaries as the sample continues to sinter through higher temperatures. X-ray diffraction and examination of the 17-4PH stainless steel phase diagrams indicate that this phase is δ-ferrite [16]. The presence of this phase seems to aid a more rapid decrease in porosity as is witnessed by the elimination of porosity preferentially at the pores surrounded by δ-ferrite.

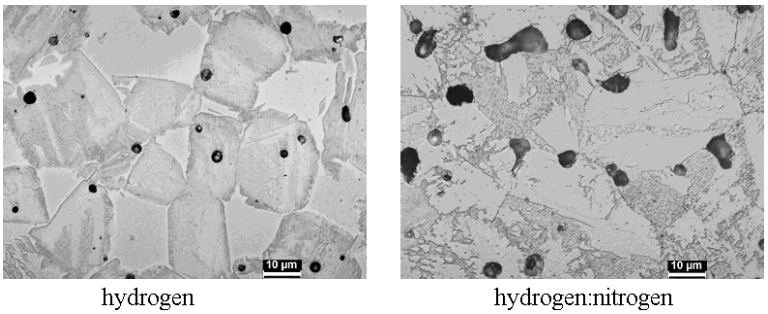

Figure 6: Microstructures of die-compacted samples quenched after sintering for 1 hour at 1365 °C in both pure H_2 and the H_2:N_2 mixture.

Comparison of the final microstructures of the die-compacted samples sintered in H_2 and H_2:N_2 after the 1 hour hold at 1365 °C show large quantities of retained austenite in the H_2:N_2 samples, Figure 6. The H_2:N_2 sample also shows no presence of the δ-ferrite phase, and contains significantly larger amounts of porosity. This supports the hypothesis that presence of the δ-ferrite phase

is crucial for obtaining high density, and indicates that sintering in the presence of nitrogen is not favourable for high density.

5 Conclusions

The sintering kinetics of die-compacted and PIM 17-4PH stainless steel have been explained through use of sintering shrinkage data and microstructural analysis. If 17-4PH is sintering in a pure hydrogen environment, δ-ferrite forms above $1220\,^{\circ}\mathrm{C}$. This phase significantly aids densification as it forms along the pore boundaries and eliminates porosity more rapidly. Nitrogen acts as an austenite-stablizer for 17-4PH. The denser austenite retards the shrinkage rate and slows densification. It also prevents the favourable δ-ferrite phase from forming, further retarding densification. This information lends important insight to the sintering mechanism of 17-4PH stainless steel. It can be used to design optimal sinter cycles and in programming of sinter models.

6 Acknowledgements

This work was performed under the financial support of the NIST/ATP Program "Powder Metal Injection Molding", Grant No. 70NAN-BOH3019.

References

[1] R.M. German and A. Bose. *Injection Molding of Metals and Ceramics*. Metal Powder Industries Federation, Princeton, NJ, 1997.

[2] J.R. Davis. *Stainless Steels*. ASM International, Materials Park, OH, 1994.

[3] H. Zhang and R.M. German. Proceedings 1992 powder injection molding symposium. pages 219–227, Princeton, NJ, 1992. Metal Powder Industries Federation.

[4] S. Banerjee. In P.H. Booker, J. Gaspervich, and R.M. German, editors, *Proceedings of 1992 Powder Injection Molding Symposium*, pages 181–192, Princeton, NJ, 1992. Metal Powder Industries Federation.

[5] R.M. German and D. Kubish. *International Journal of Powder Metallurgy*, 29:47–62, 1993.

[6] T. Baba, H. Miura, T. Honda, and Y. Tokuyama. In M. Philips and J. Porter, editors, *Advances in Powder Metallurgy and Particulate Materials*, volume 2, pages 6.271–6.278, Princeton, NJ, 1995. Metal Powder Industries Federation.

[7] J.J. Valencia, T.J. McCabe, and H. Dong. In M. Philips and J. Porter, editors, *Advance in Powder Metallurgy and Particulate Materials*, volume 2, pages 6.205–6.212, Princeton, NJ, 1995. Metal Powder Industries Federation.

[8] H. Kyogoku, S. Komatsu, H. Nakayama, H. Jinushi, and K. Shinohara. In R.A. McKotch and R. Webb, editors, *Advances in Powder Metallurgy and Particulate Materials*, volume 3, pages 13.135–18.144, Princeton, NJ, 1997. Metal Powder Industries Federation.

[9] J.J. Valencia and J.R. Spirko. In F.H. Froes and J. Hebeisen, editors, *Advanced Particulate Materials and Processes*, pages 411–419, Princeton, NJ, 1997. Metal Powder Industries Federation.

[10] J.W. Newkirk, J.A. Sago, and G.M. Brasel. In T.S. Srivatan and K.A. Khor, editors, *Processing and Fabrication of Advanced Materials VII*, pages 213–223, Warrendale, PA, 1998. TMS.

[11] K.A. Green. In J.J. Oakes and J.H. Reinshagen, editors, *Advances in Powder Metallurgy and Particulate Materials*, volume 2, pages 5.119–5.130, Princeton, NJ, 1998. Metal Powder Industries Federation.

[12] E.A. Olevsky. Theory of sintering: From discrete to continuum. *Materials Science and Engineering*, R23:41–100, 1998.

[13] E.A. Olevsky and R.M. German. Effect of gravity on dimensional change during sintering - i. shrinkage anisotropy. *Acta Materialia*, 48:1153–1166, 2000.

[14] E.A. Olevsky and R.M. German. Effect of gravity on dimensional change during sintering - II. shape distortion. *Acta Materialia*, 48:1167–1180, 2000.

[15] R.M. German. *Sintering Theory and Practice*. John Wiley and Sons, New York, NY, USA, 1996.

[16] Y. Wu, D. Blaine, B. Marx, C. Schlaefer, and R.M. German. Sintering densification and microstructure evolution of injection molding grade 17-4 PH stainless steel powder. *Metallurgical and Materials Transactions*, 33, 2002.

[17] Y. Wu, R.M. German, D. Blaine, C. Schlaefer, and B. Marx. Effects of residual carbon content on sintering shrinkage, microstructure and mechanical properties of injection molded 17-4 PH stainless steel. *Journal of Materials Science*, 37:1–11, 2002.